

Contents

List of Figures	3
List of Tables	3
1 Abstract	4
2 Model Flow Chart	5
3 Arm Properties	6
3.1 PCSA, Optimal Length, and %FT	6
3.2 Model Variations	6
3.3 Forearm Moment of Inertia	7
4 Targets and reaching direction	7
5 Minimum Jerk	8
6 Inverse Kinematics	9
7 Inverse Dynamics	9
7.1 Alaa's Method	10
7.2 Effective Mass Calculation	10
8 Muscle Moment Arms and Lengths	13
8.1 Muscle Moment arms - 8 Muscle Model	13
8.2 Muscle Lengths - 8 Muscle Model	13
9 Force-length/velocity properties	15
10 Activation Dynamics	17
11 Forward Simulation	18
12 Umberger Energy Model	19
12.1 Mechanical Muscle Model	20
12.1.1 Hill Constants	20
12.1.2 Activation Dynamics	20
12.1.3 Mechanical to thermal energy estimates	20
12.2 Energy Expenditure Model	21
12.2.1 Activation and Maintenance Heat Rate	21
12.2.2 Shortening Muscle	21
12.2.3 Lengthening Muscle	21
12.2.4 Mechanical Work Rate	21
12.2.5 Scaling Factors	22
12.3 Total Energy Rate	22
13 Metabolic Methods	22
14 Model Fitting	23
15 Results	23

List of Figures

1	Diagram of the 8 simulated muscles and which muscles they represent.	7
2	Target Orientation from start position (home).	8
3	End point velocity using minimum jerk and speeds provided in Table 3.	9
4	Inverse dynamics and plotted shoulder/elbow position, torque, and acceleration. All plots are for the masses fastest speed, and towards target A, for a distance of 10 cm.	11
5	Effective mass calculation separated by target and condition for the 3rd speed for each respective mass. In each subplot yellow is 20 lbs added, green is 10 lbs, blue is 5 lbs, purple is 0 lbs added. The initial and final values are shown in the text.	12
6	Muscle moment arms and lengths.	14
7	All plots are done at an activation level of 1. A. Normalized Tension as a function of current length and velocity. B. Force Velocity parameter. C. Force length parameter. C. Passive force element, the passive element is flipped, as short length it uses a negative force and at long lengths 0 to simulate long lengths having higher force than shorter lengths.	16
8	Activation dynamics as used from Li and Todorov. $t_{ACT} = 50$ msec, and $t_{DEACT} = 66$ msec.	17
9	A. The active state of the muscles given a neural drive of one. We only see one line here as all the muscles obey the same activation dynamics (10). This could be changed to use the umberger model where we would see slight differences in activation dynamics (12.1.2). B. The force output of each muscle given the force-length and force-velocity parameters (9) C. Torques supplied by the muscles using moment arm x force (8.1). Solid lines are torques about the elbow, dashed lines about the shoulder. D Total torques about each joint.	18
10	A. The active state of the muscles given a neural drive of one. The activation dynamics are from the umberger model so we see slight differences in activation times (10). This could be changed to use the umberger model where we would see slight differences in activation dynamics (12.1.2,12.1.2). B. The force output of each muscle given the force-length and force-velocity parameters (9) C. Torques supplied by the muscles using moment arm x force (8.1). Solid lines are torques about the elbow, dashed lines about the shoulder. D Total torques about each joint.	19
11	R^2 value as a function of minimization parameter and predictor variable for a linear fit.	24
12	R^2 value as a function of minimization parameter and predictor variable for an exponential fit.	25
13	A. Model compared to metabolic cost with R^2 and model fit equation. B. The model fit compared to the collected metabolic cost.	26

List of Tables

1	Properties of the forearm and upperarm rigid segments. The values for Forearm $Cent_L$ and I_{COM} are for 0 added mass at the hand.	6
2	Muscle Properties. For L_{OPT} , the letter corresponds to which author the value was taken from. C[1], L[2], M[3].	6
3	Movement times averaged across targets for given masses.	9
4	Coefficients for polynomial fits to moment arm lengths.	13
5	Coefficients for polynomial fits to moment arm lengths.	14
6	Activation and deactivation times using the Umberger Model	17

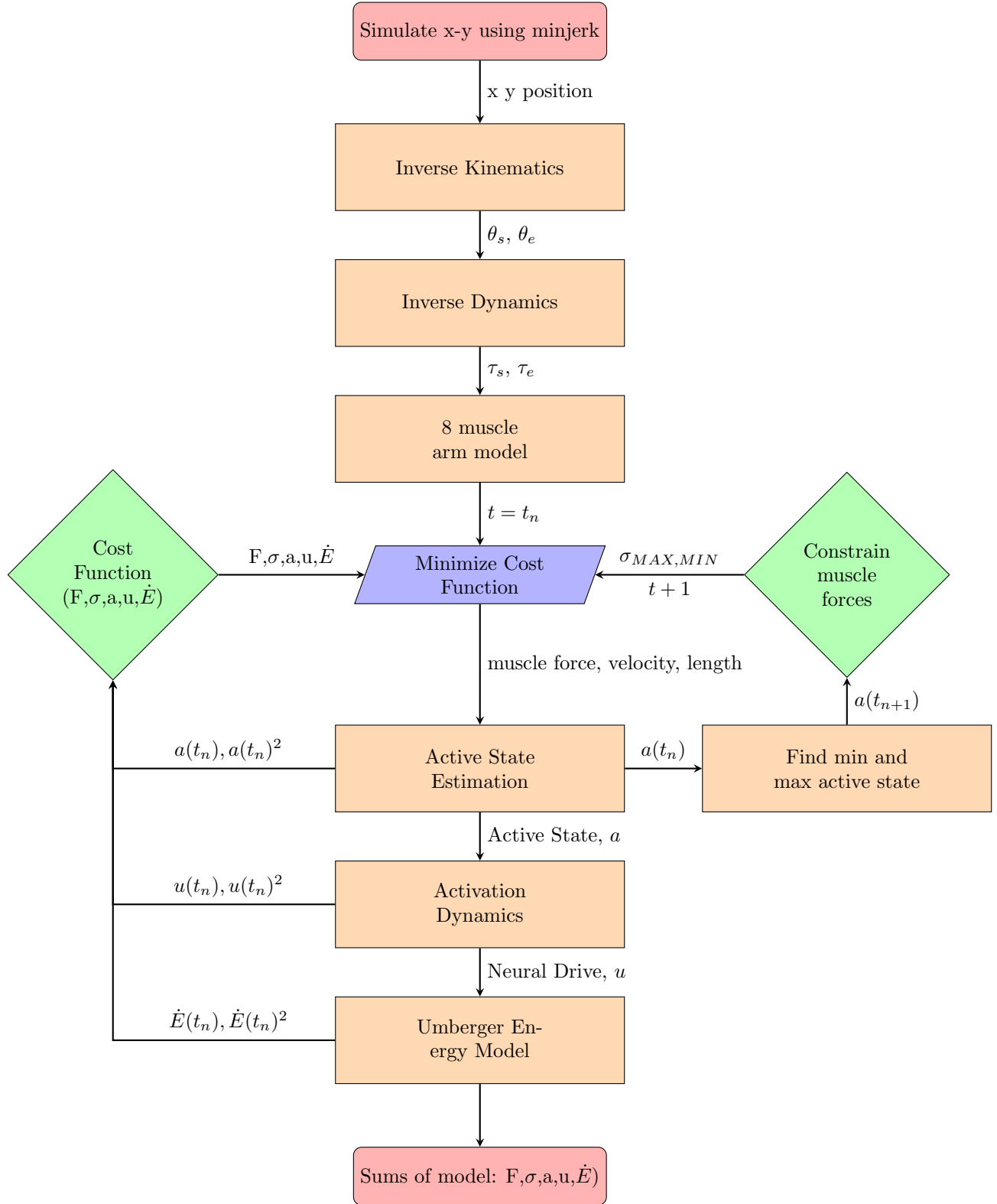
1 Abstract

Intro: The cost of making a movement has been proposed as a main driving force in determining movement characteristics such as speed and accuracy. Estimates for the cost of movement, like joint torque and neural drive, have been used in many arm reaching studies. It is unclear however how many of these estimates correlate to the actual cost of arm reaching movements. We examine how five different estimates, joint torque, muscle force, muscle active state, neural drive, and an estimate for metabolic cost, relate to the metabolic cost of arm reaching.

Methods: We developed a biomechanically accurate model of the arm that we use to estimate multiple biomechanical variables and then relate them to metabolic cost of arm reaching from collected subject data. Metabolic rate of arm reaching was collected from eight subjects that made 10 cm reaches. Subjects made reaches to four different targets oriented at 45, 135, 225, and 315 degrees from the right horizontal. 0, 5, 10, and 20 lbs of mass were added to the hand. Reaches were made in one of 6 time windows ranging from 0.45 seconds to 1.35 seconds. The biomechanical model of the arm consists of two joints (shoulder and elbow), two arm segments (upperarm and forearm), and eight muscles. It makes planar reaching movements from a minimum jerk trajectory using movement times from the metabolic data. Using inverse dynamics the model calculates joint torques from the trajectory to four simulated targets with four different added masses at the hand. The model then tests multiple minimization functions to distribute muscle force across the eight muscles. Once muscle force has been determined it calculates muscle active state and determines neural drive to the muscle. Last a model for energetic expenditure is used for an estimate of metabolic cost of the specific reach. We then integrated the time-series data for joint torque, muscle force, muscle active state, neural drive, and estimated metabolic cost for each mass and speed condition and fit these sums to collected metabolic data using either a linear or quadratic function. R² values are computed from the fits and used as a metric of accuracy.

Results: Using a minimization function of stress and a linear fit the best fit to measured metabolic cost was the energy expenditure model with an R² value of 0.71 with a function $3.25x - 25.11$. A common function for estimating cost of arm reaching, joint torque rate squared, only had an r-squared value of 0.49. By testing multiple minimization functions we find that the specific model function has an effect of the model fits. When using these types of simulations for modeling decision making we must be careful only using an estimate of metabolic cost as we also show that metabolic cost is not the only thing driving movement decisions. Certain biomechanical variables from these simulations may be able to accurately represent the metabolic cost of the movement.

2 Model Flow Chart



3 Arm Properties

The properties of forearm centroid length and I_{COM} change depending on the amount of mass added to the hand. The arm lengths and masses are relatively similar to a few papers [4, 5].

Object	Mass (kg)	Length (m)	$Cent_L$ (m)	I_{com}
Forearm	1.1586	0.429	0.286	0.01882
Upperarm	1.9328	0.33	0.165	0.0141

Table 1: Properties of the forearm and upperarm rigid segments. The values for Forearm $Cent_L$ and I_{COM} are for 0 added mass at the hand.

These muscle parameters are estimated from muscle lengths and cross sectional areas and the density of the muscle.

Muscle	Mass (kg)	PCSA (m^2)	L_{OPT}	% FT
Anconeus (AN)	0.0291	4E-4	0.0687 (C)	40.0
Brachialis (BS)	0.0829	8.71E-4	0.090 (L)	40.0
Brachioradialis (BR)	0.0525	2.95E-4	0.1887 (L)	60.2
Deltoid Anterior (DA)	0.1005	5.46E-4	0.1296 (L)	42.9
Deltoid Posterior (DP)	0.1323	5.69E-4	0.1818 (L)	42.9
Pectoralis (PC)	0.0816	6.68E-4	0.1701 (L)	57.0
Biceps Brachii(BB)	0.1278	4.32E-4	0.225 (M)	53.6
Triceps Brachii (TB)	0.3920	11.94E-4	0.3235 (M)	52.9

Table 2: Muscle Properties. For L_{OPT} , the letter corresponds to which author the value was taken from. C[1], L[2], M[3].

3.1 PCSA, Optimal Length, and %FT

The muscle masses can be computed using $mass = L_{OPT} \cdot PCSA \cdot \rho$ where ρ is $10.6 \text{ kg}/\text{m}^3$. The PCSA for each muscle is estimated from cadaver studies [2, 6]. The cross sectional area for the brachioradialis is taken from [7]. The cross sectional areas are all increased by 1 as it was needed for the muscles to be strong enough for the faster movements. The $PCSA$ for each muscle can be estimated similar to the Todorov model [8], or from cadaver studies done by Holzbaur and Murray by dividing the muscle volume by the optimal fiber length [9, 3].

Currently the model uses the optimal muscle lengths from Murray [3] and combining the heads of muscles. Some of these values are taken from Langenderfer [2] as Murray does not test them. However, Chang et al.[1] shows that the optimal lengths of the muscles are quite a bit shorter than reported by Langenderfer and Murray. I think the optimal muscle lengths for the brachialis should agree more with the shorter values in Chang[1] as these values match up closer to Pigeon[10] and Van Zuylen[11].

If not listed it assumes the optimal fiber lengths occur at 45° shoulder flexion and 90° elbow flexion, and that the length of the muscle at that position is given in equation 12. This method may not be accurate for some muscles as they would vary greatly if the equation is used when compared to the Langenderfer model. Kistemaker shows 5 references that show that the optimal elbow flexor angle to maximize the elbow moment is also 45° [12].

Percent fast twitch of each of the muscles can be estimated from [13, 14]. For data that has deep and superficial values an average is taken for percent fast twitch.

3.2 Model Variations

There are two working models. One model uses 6 muscles that are similar to Li and Todorov [8]. The length properties could be scaled to the optimal fiber length parameter in previous literature as the current lengths do not

account for tendon lengths [9, 2]. I'm not sure how much changing the total length of the muscle will affect the active state properties of the muscles in 14 [15]. If this method does not work then the model would need to determine the length of each muscle plus the tendon to get an accurate measure of the length of the muscle.

The second model uses 8 arm muscles that are defined from cadaver studies [10]. The second model is the one currently being used as it gives functions for moment arms and muscle lengths as a function of shoulder and elbow angle. Murrary, Pigeon, Delp, and Kistemaker all provide models for muscle lengths, but I'm leaning towards using Pigeon's model because it provides easily accesible equations [16, 10, 17, 18].

A diagram of the six muscle model and their locations is shown in Figure 1 [8, 17].

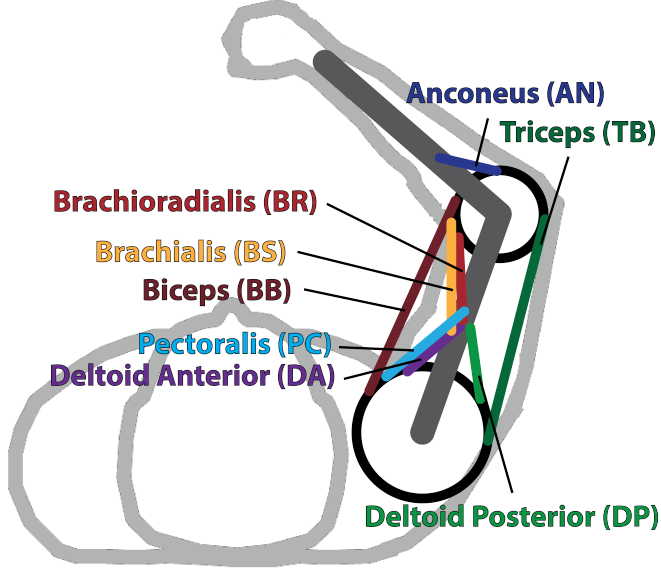


Figure 1: Diagram of the 8 simulated muscles and which muscles they represent.

3.3 Forearm Moment of Inertia

To find the new moment of inertia about the center of mass of the forearm plus added mass we need to use the parallel axis theorem.

$$Cent_{L,new} = \frac{Cent_{L,old} \cdot m_2 + l_2 \cdot (\text{mass added})}{m_2 + \text{mass added}} \quad (1)$$

$$I_{com,new} = 0.01882 + m_2(Cent_{L,old} - Cent_{L,new})^2 + \text{added mass}(l_2 - Cent_{L,new})^2$$

4 Targets and reaching direction

The simulation was set to reach towards four different targets located at 45° , 135° , 225° , and 315° from the right horizontal (Figure 2). The targets were also spaced at 5 cm, 10 cm, 15 cm, and 20 cm. Figure 2 shows the setup for the targets. The starting position of the hand was set to be $x = -7.58$ cm and $y = 48.78$ cm. The targets were then placed at the distances and directions specified before.

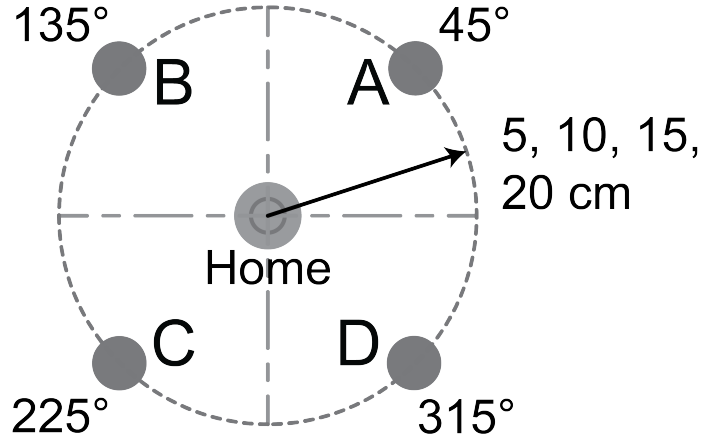


Figure 2: Target Orientation from start position (home).

5 Minimum Jerk

Minimum Jerk trajectory is an approximation of the position, velocity, and acceleration of the hand position when making an arm reaching movement. This was used to simulate reaches to 4 different targets positioned at 45°, 135°, 225°, 315° from the right horizontal. Humans have been shown to reach approximately in a manner that minimizes the jerk of the motion in a straight line [19].

Minimum jerk minimizes the function:

$$H(x(t)) = \frac{1}{2} \int_{t_0}^{t_f} \dot{x}^2 dt \quad (2)$$

Solving this function provides x , \dot{x} , and \ddot{x} .

$$\begin{aligned} x &= a_0 + a_1 t + a_2 t^2 + a_3 t^3 + a_4 t^4 + a_5 t^5 \\ \dot{x} &= a_1 + 2a_2 t + 3a_3 t^2 + 4a_4 t^3 + 5a_5 t^4 \\ \ddot{x} &= 2a_2 + 6a_3 t + 12a_4 t^2 + 20a_5 t^3 \end{aligned} \quad (3)$$

Knowing initial and final conditions we are able to solve for the constants $a_1 \dots a_6$. Using $x(0) = 0$, $\dot{x}(0) = 0$, $\ddot{x} = 0$, we can solve a_0 , a_1 , $a_2 = 0$.

Or in a more simple form, if we are moving from x_i to x_f in $t = d$, the minimum jerk equation is showing in Eq. 4. This can be solved in both x and y directions to compute the x and y position data.

$$\begin{aligned} x(t) &= x_i + (x_f - x_i) \left(10 \left(\frac{t}{d} \right)^3 - 15 \left(\frac{t}{d} \right)^4 + 6 \left(\frac{t}{d} \right)^5 \right) \\ \dot{x}(t) &= (x_f - x_i) \left(30 \left(\frac{t}{d} \right)^2 - 60 \left(\frac{t}{d} \right)^3 + 30 \left(\frac{t}{d} \right)^4 \right) \\ \ddot{x}(t) &= (x_f - x_i) \left(60 \left(\frac{t}{d} \right) - 180 \left(\frac{t}{d} \right)^2 + 120 \left(\frac{t}{d} \right)^3 \right) \end{aligned} \quad (4)$$

The speed with which the model was simulated depended on the mass added (Table 3). During subject testing the heaviest mass condition was not able to be moved at the highest speed without fatigue so we tested slower speeds for the two heavier masses. The speeds are shown in table Using these equations and the times specified in our testing protocol we get velocity traces that look similar to Figure 3.

Mass	Time 1	Time 2	Time 3	Time 4	Time 5	Time 6
0 lbs	0.4407	0.492	0.5908	0.7733	0.9650	1.1567
5 lbs	0.4703	0.5089	0.5856	0.7807	0.9694	1.1657
10 lbs	0.5114	0.6006	0.7847	0.9701	1.1591	1.3438
20 lbs	0.5301	0.6049	0.7849	0.9756	1.1634	1.3371

Table 3: Movement times averaged across targets for given masses.

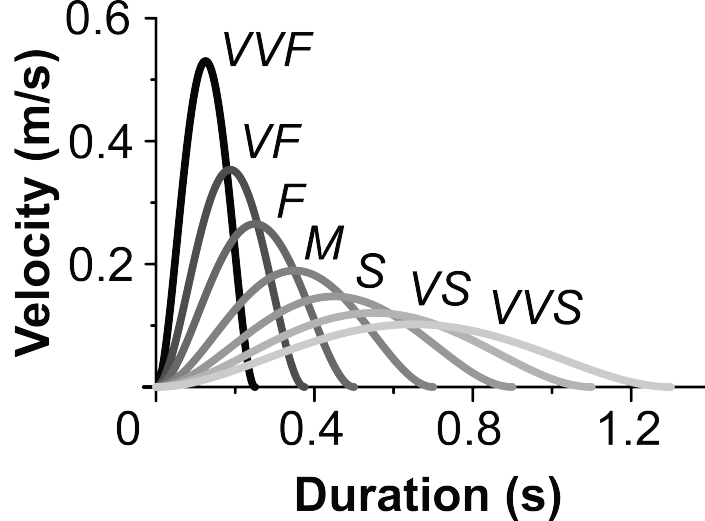


Figure 3: End point velocity using minimum jerk and speeds provided in Table 3.

6 Inverse Kinematics

The first step is to convert the data (in x and y position data) to joint positions θ_e and θ_s . These angles are defined by their Euler Angles and not flexion extension angles. From there we differentiate to get the angular velocities $\dot{\theta}_e$ and $\dot{\theta}_s$. In these equations l_1 and θ_s refer to the upper arm segment and shoulder joint. l_2 and θ_e refer to the forearm and elbow joint. For a more indepth derivation see [20].

$$\begin{aligned} \theta_e &= \text{atan2} \left(\pm \sqrt{1 - \left(\frac{x^2 + y^2 - l_1^2 - l_2^2}{2l_1l_2} \right)^2}, \left(\frac{x^2 + y^2 - l_1^2 - l_2^2}{2l_1l_2} \right) \right) \\ \theta_s &= \text{atan2}(y, x) - \text{atan2}(l_2 \sin(\theta_e), l_1 + l_2 \cos(\theta_e)) \end{aligned} \quad (5)$$

7 Inverse Dynamics

Next we differentiate the angular positions to get angular velocities and angular accelerations. From there the angular derivatives the joint torques can be derived. For an indepth derivation see [21].

$$\begin{bmatrix} \tau_s \\ \tau_e \end{bmatrix} = \begin{bmatrix} a_1 + a_4 & a_3 \cos(\theta_e - \theta_s) \\ a_3 \cos(\theta_e - \theta_s) & a_2 \end{bmatrix} \begin{bmatrix} \ddot{\theta}_s \\ \ddot{\theta}_e \end{bmatrix} + \begin{bmatrix} 0 & -a_3 \dot{\theta}_e \sin(\theta_e - \theta_s) \\ a_3 \dot{\theta}_e \sin(\theta_e - \theta_s) & a_2 \end{bmatrix} \begin{bmatrix} \dot{\theta}_s \\ \dot{\theta}_e \end{bmatrix} \quad (6)$$

$$\begin{aligned}
a_1 &= m_s |^s x_{l,cent}|^2 + I_{s,ZZ} \\
a_2 &= m_e |^e x_{l,cent}|^2 + I_{e,ZZ} \\
a_3 &= m_2 l_1 |^e x_{2e}| \\
a_4 &= m_2 l_1^2
\end{aligned} \tag{7}$$

7.1 Alaa's Method

In the following equations we define the variables as follows: m_1 = upperarm mass, r_1 = upperarm centroid length, l_1 = upperarm length, $I_{COM,1}$ = moment of inertia about its center of mass. m_2 = forearm mass, r_2 = the length to the center of mass of the forearm, r_{22} = the length to the centroid (arm + mass), l_1 = forearm length, $I_{COM,1}$ = moment of inertia about its centroid with the added mass.

This method is the same as before just a little more fleshed out, code wise it may be a little simpler or easier to read but both methods are valid.

$$\begin{aligned}
I &= \begin{bmatrix} m_1 r_1^2 + I_{COM,1} + (mass + m_2)(l_1^2 + r_{22}^2 + 2l_1 r_{22} \cos(\theta_e)) + I_{COM,2} & (m_2 + mass)(r_{22}^2 + l_1 r_{22}^2 \cos(\theta_e)) + I_{COM,2} \\ (m_2 + mass)(r_{22}^2 + l_1 r_{22}^2 \cos(\theta_e)) + I_{COM,2} & m_2 r_2^2 + mass \cdot l_2^2 + I_{COM,2} \end{bmatrix} \\
C &= \begin{bmatrix} -m_2 r_{22} l_1 \dot{\theta}_e^2 \sin(\theta_e) - 2m_2 r_{22} l_1 \dot{\theta}_s \dot{\theta}_e \sin(\theta_e) \\ m_2 r_{22} l_1 \dot{\theta}_s^2 \sin(\theta_e) \end{bmatrix} \\
\begin{bmatrix} \tau_s \\ \tau_e \end{bmatrix} &= I \cdot \begin{bmatrix} \ddot{\theta}_s \\ \ddot{\theta}_e \end{bmatrix} + C
\end{aligned} \tag{8}$$

Figure 4 shows the results of an inverse dynamics simulation towards target

7.2 Effective Mass Calculation

The effective mass is used to estimate the arms resistance to a force in a given direction[4]. To determine the effective mass of the arm at a given time point we need to define a Jacobian matrix Λ .

$$\Lambda = \frac{dx}{d\theta} = \begin{bmatrix} -l_1 \sin(\theta_s) - l_2 \sin(\theta_s + \theta_e) & -l_2 \sin(\theta_s + \theta_e) \\ l_1 \cos(\theta_s) + l_2 \cos(\theta_s + \theta_e) & l_2 \cos(\theta_s + \theta_e) \end{bmatrix} \tag{9}$$

The inertia matrix is the same as defined above in section 7.1, Eq. 8, variable M. Then defining the mass matrix as:

$$M = (\Lambda^{-1})^T I(\theta) \Lambda^{-1} \tag{10}$$

Last we induce a force of 1 in the reach direction to compute the effective mass of the reaching movement. In Eq. 11, θ is the angle of reaching direction, and +1 is added at the end to account for the inertia of the robotics arm manipulandum.

$$\text{Effective mass} = \text{norm}(M * [\cos(\theta) \quad \sin(\theta)]) + 1 \tag{11}$$

The effective mass as a function of target, mass added, and distance is shown in Figure 5. In this equation θ is the movement direction from the right horizontal. It would be equivalent to Figure 2.

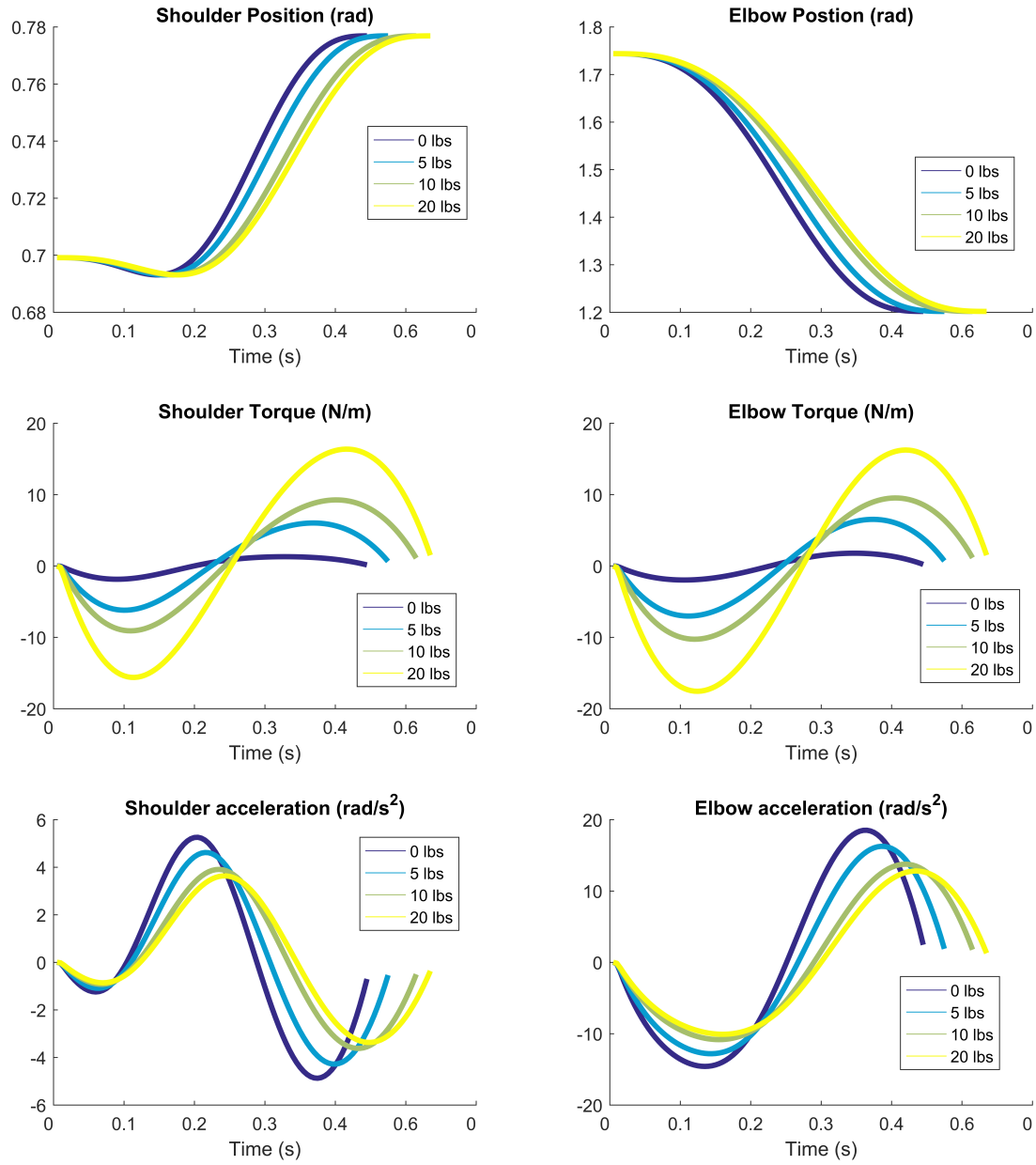


Figure 4: Inverse dynamics and plotted shoulder/elbow position, torque, and acceleration. All plots are for the masses fastest speed, and towards target A, for a distance of 10 cm.

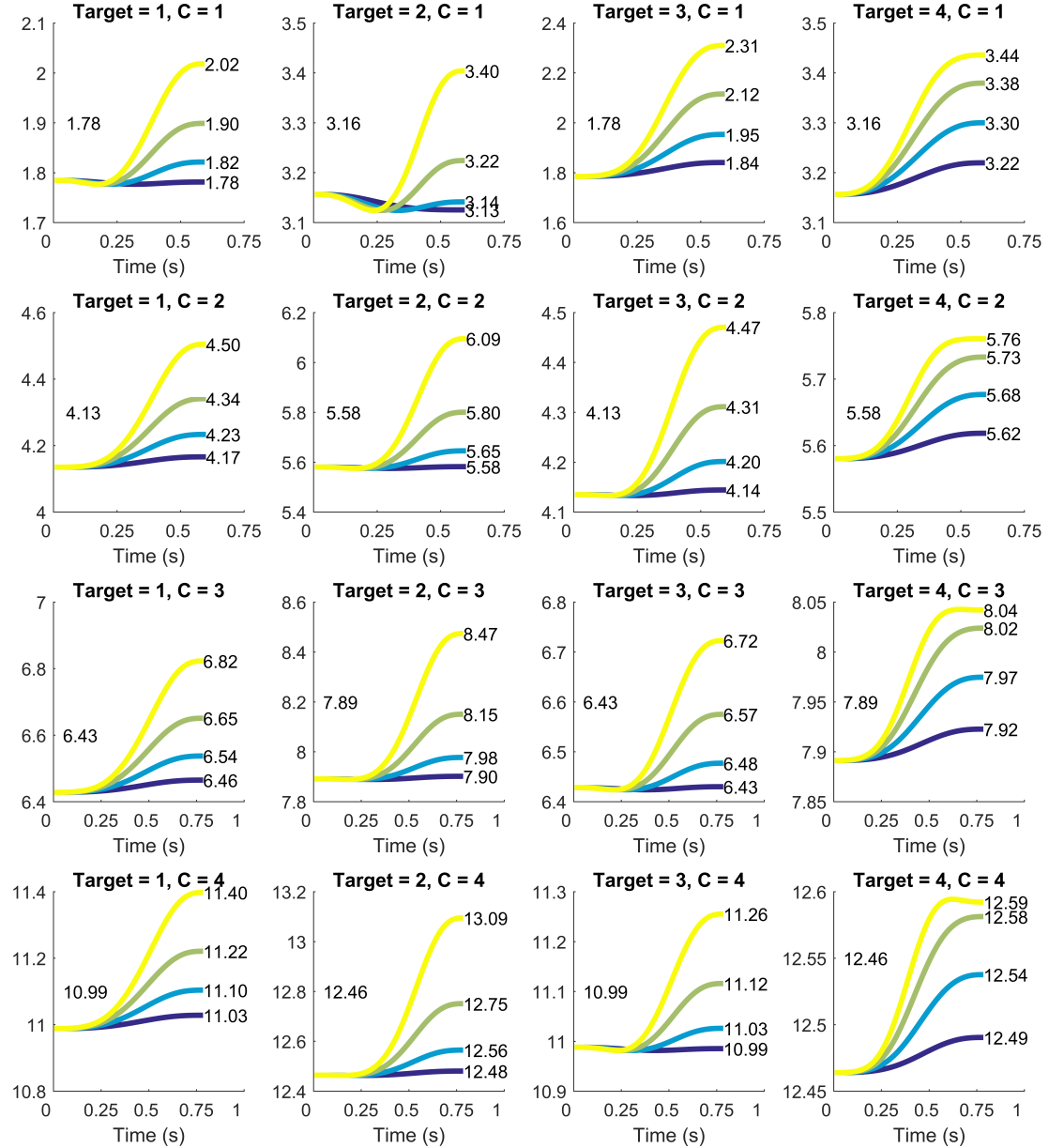


Figure 5: Effective mass calculation separated by target and condition for the 3rd speed for each respective mass. In each subplot yellow is 20 lbs added, green is 10 lbs, blue is 5 lbs, purple is 0 lbs added. The initial and final values are shown in the text.

8 Muscle Moment Arms and Lengths

8.1 Muscle Moment arms - 8 Muscle Model

The moment arms were set to vary with shoulder and elbow position as defined below [10]. Another approximation could be used from cadaver studies by Murray [16] but it may not have all the muscles needed. A negative moment arm is used to provide a negative torque around the joint as muscle force can never be less than 0.

The Pigeon model fits polynomials to the moment arm and muscle lengths as a function of shoulder and elbow angle. A graph showing how the moment arms are changing is shown in figure 6a.

$$MA = x_n q_j^n + x_{n-1} q_j^{n-1} + \cdots + x_1 q_j + x_0$$

$$ML = cst + \sum_{j=1}^3 (Y_n q_j^n + y_{n-1} q_j^{n-1} + \cdots + y_1 q_j) \quad (12)$$

The coefficients for this equation is shown in the tables below. Most of the coefficients are scaled to a power of 10.

DF	Moment Arm Coefficients					
	Elbow flexion/extension				Shoulder F/E	
Muscle	$c_5 \times 10^9$	$c_4 \times 10^7$	$c_3 \times 10^5$	$c_2 \times 10^3$	$c_1 \times 10^1$	c_0
AN	-2.7306	10.448	-14.329	8.4297	-2.2841	-5.3450
BS			-2.0530	2.3425	2.3080	5.5492
BR			-6.5171	10.084	1.6681	19.490
DA						33.02
DP						-78.74
PC						50.80
BB			-2.9883	1.8047	4.5322	14.660
TB	-3.5171	13.277	-19.092	12.886	-3.0284	-23.287
						-25.40

Table 4: Coefficients for polynomial fits to moment arm lengths.

8.2 Muscle Lengths - 8 Muscle Model

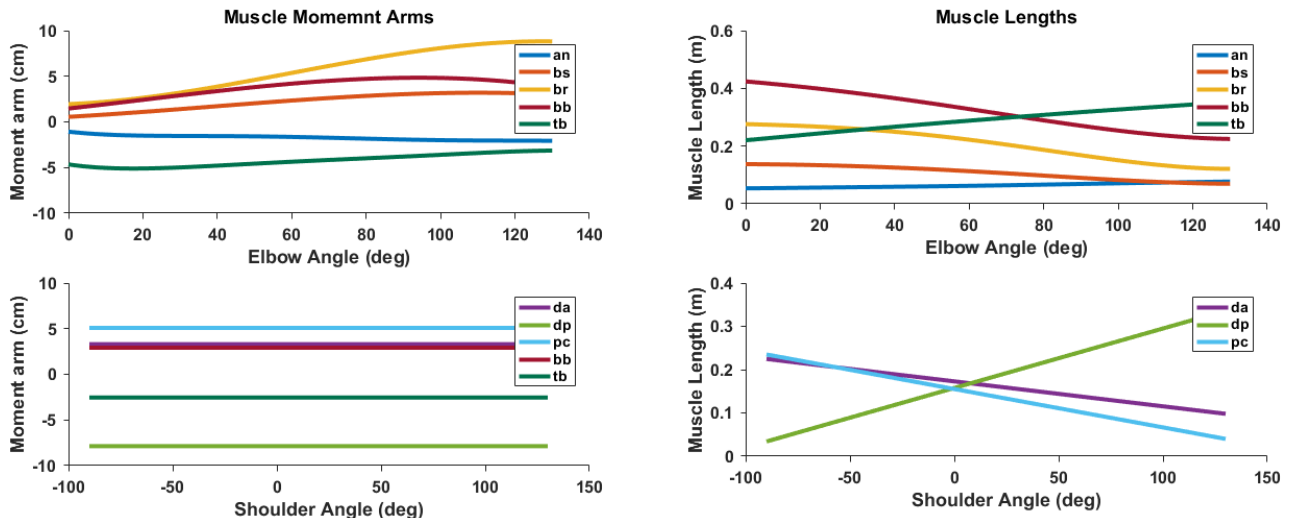
The optimal lengths of the muscles as shown in table 2 were estimated with the arm in a neutral position where $\theta_s = 45^\circ$ and $\theta_e = 90^\circ$. The following equations describe how I calculate the lengths of the muscles. They are solved for in a similar way to moment arms [10]. A graphical representation of the muscle lengths is shown in figure 6b.

Kistemaker used cadaver studies to estimate the muscle lengths, though I'm not sure how they actually measured the muscle lengths as there were not equations or parameters set for the model [12, 16, 18].

Muscle Length Coefficients

Muscle	$cst(\text{mm})$	Elbow flexion/extension						$u_1 \times 10^1$
		$t_6 \times 10^{11}$	$t_5 \times 10^8$	$t_4 \times 10^7$	$t_3 \times 10^5$	$t_2 \times 10^3$	$t_1 \times 10^2$	
AN	53.57	4.7658	-1.8235	25.008	-14.713	3.9865	9.3288	
BS	137.48			3.5832	-4.0884	-4.0282	-9.6852	
BR	276.13			11.374	-17.600	-2.9114	-34.017	
DA	172.84							-5.7631
DP	157.64							13.743
PC	155.19							-8.8663
BB	378.06			5.2156	-3.1498	-7.9101	-25.587	-5.0981
TB	260.05	6.1385	-2.3174	33.321	-22.491	5.2856	40.644	4.4331

Table 5: Coefficients for polynomial fits to moment arm lengths.



(a) Muscle moment arms as a function of shoulder or elbow angle.

(b) Muscle lengths as a function of joint angle (deg).

Figure 6: Muscle moment arms and lengths.

9 Force-length/velocity properties

The model used is the Brown, Cheng and Loeb model [15]. Other models can also be used such as cross-bridge cycling models [22, 23] or hill type models [24, 12, 25, 26]. The Brown model accounts for active and passive elements of the muscle tendon unit. l is defined as the normalized length l/l_{OPT} , v is in normalized units of L_{OPT}/s . Activate state (a) is computed using Eq. 14. $F_{p,1}$ is the passive force resisting tension. $F_{p,2}$ is the passive force resisting compression of the muscle.

The basic form of these equations is

$$\begin{aligned} F_{PE} &= F_{p,1} + R * A_f * F_{p,2} \\ F_{CE} &= R * A_f * F_L * F_V \\ F_{total} &= F_{PE} + F_{CE} \end{aligned} \quad (13)$$

Which simlifies to

$$F_{total} = F_{p,1} + R * A_f (F_L * F_V + F_{p,2})$$

$$\begin{aligned} F_{p,1} &= 68.35 * 0.0495 * \log(\exp((l - 1.445)/(0.0495)) + 1) \\ F_{p,2} &= -0.02\exp(13.8 - 18.7l) \\ F_v &= \begin{cases} \frac{-5.72-v}{-5.72+v(1.38+2.09l)} & v \leq 0 \\ \frac{0.62-v(-3.12+4.21*l-2.67l^2)}{0.62v} & v > 0 \end{cases} \\ F_l &= \exp\left(-\left|\frac{l^{1.93}}{1.03}\right|^{1.87}\right) \\ N_f &= 2.11 + 4.16\left(\frac{1}{l} - 1\right) \\ A &= \frac{T - F_{p,1}}{F_l F_v + F_{p,2}} \\ a &= 0.56N_F 10^{\log_{10}(1-A)/N_f} \end{aligned} \quad (14)$$

The passive force from the muscles, at the lengths we have should never really get about 5 N [27]. This passive force is subtracted form the total joint torque to solve for the active compoments of force that the muscles need to produce.

Once the active state is calculated, it is scaled by a normalized force ($\sigma = 31.8 \text{ N/m}^2$) [8] to get muscle force. This value may be low as the maximum isometric forces generated by the muscles are much lower than shown in previous studies [28]. It has been shown that for simulation purposes this value may need to be as high as 100 N/m^2 for simulation [29]. For this model it is set to 200 N/m^2 .

$$F = a \cdot \sigma \cdot A, \quad \text{where } A \text{ is area} \quad (15)$$

The passive force properties of the muscles seem to line up relatively well with Horowitz [30]. He reports at long sarcomere lengths the human muscles produce about $0.2\text{-}0.3 \text{ kg/cm}^2$. The biceps brachii at its longest length was producing about 0.35 kg/cm^2 .

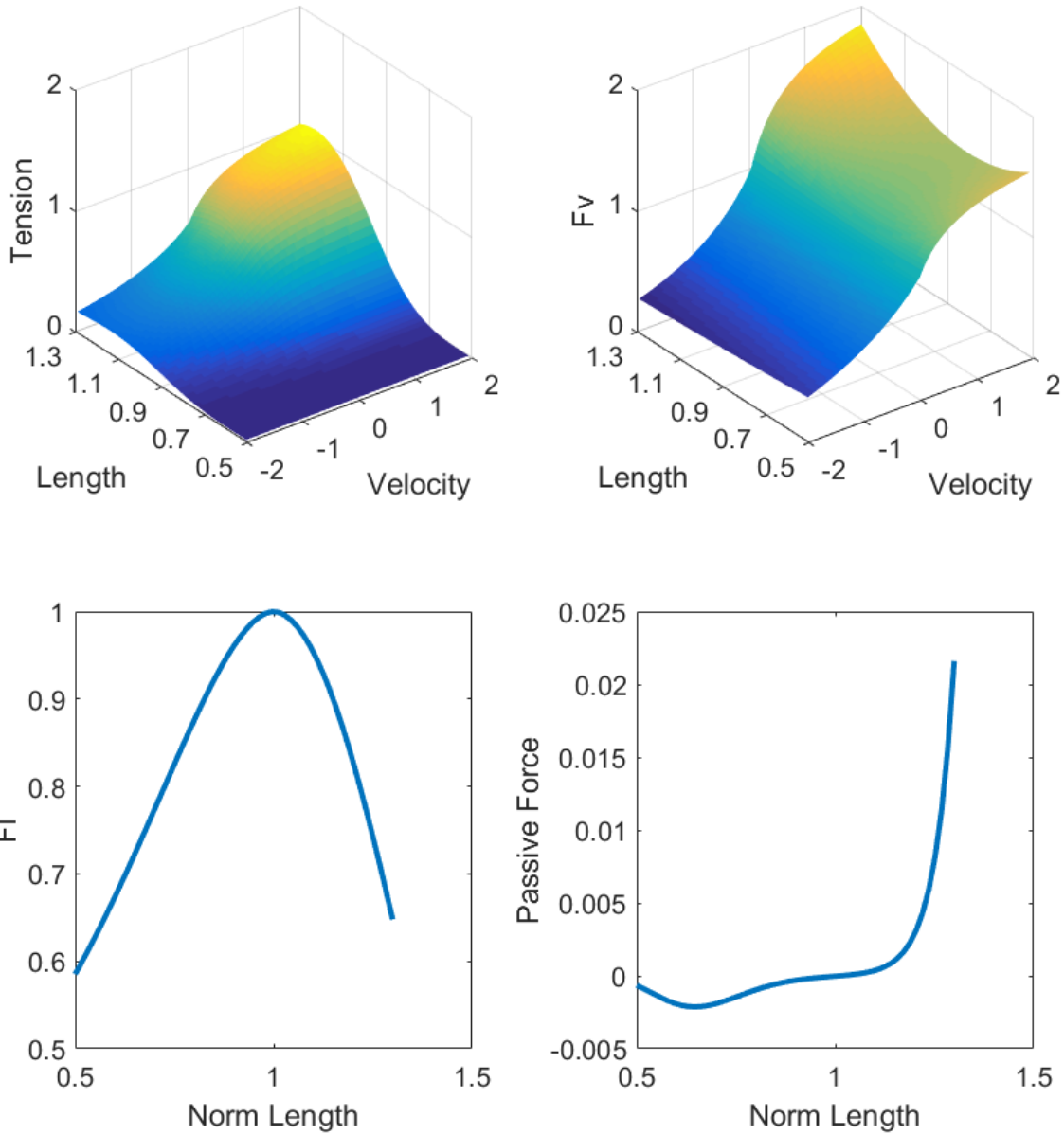


Figure 7: All plots are done at an activation level of 1. **A.** Normalized Tension as a function of currenty length and velocity. **B.** Force Velocity paramter. **C.** Force length parameter. **C.** Passive force element, the passive element is flipped, as short length it uses a negative force and at long lengths 0 to simulate long lengths having higher force than shorter lengths.

10 Activation Dynamics

The active state is estimated from neural drive by passing u (neural drive) through a filter that describes calcium dynamics [8]. It is approximated using a first order non-linear filter. This is similar to other methods [31, 32, 15].

$$\dot{a} = \frac{(1 + \sigma_u \epsilon)u - a}{t(u, a)}$$

$$t(u, a) = \begin{cases} t_{deact} + u(t_{act} - t_{deact}) & u > a \\ t_{deact} & otherwise \end{cases} \quad (16)$$

σ and ϵ represent noise in the neural drive signal. Currently I have 0 zero noise added to the signal. $t_{ACT} = 50$ msec, and $t_{DEACT} = 66$ msec.

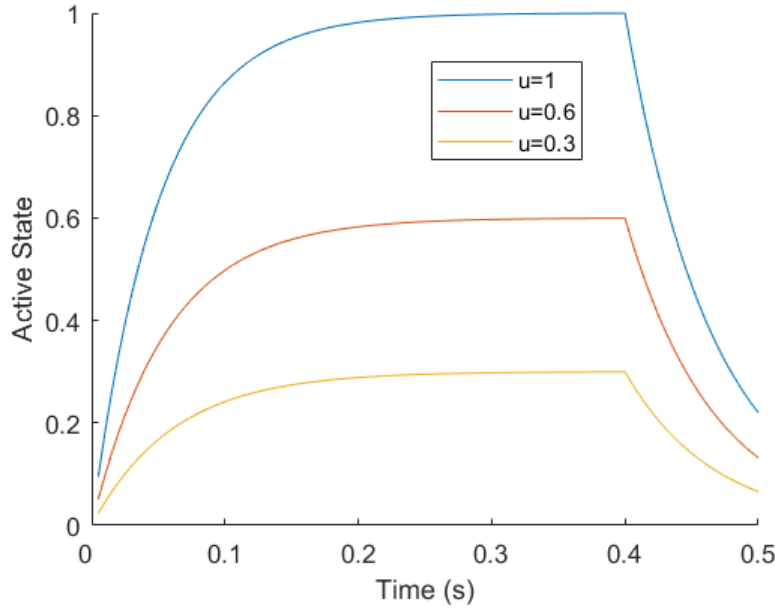


Figure 8: Activation dynamics as used from Li and Todorov. $t_{ACT} = 50$ msec, and $t_{DEACT} = 66$ msec.

The Umberger model uses different activation parameters which is shown in Eq. 18 [33]. Using our muscle parameters of %FT we would get activation and deactivation times shown in table 6.

Muscle	%FT	t_{ACT} (ms)	t_{DEACT} (ms)
1	50.3	56.36	61.83
2	42.9	59.84	65.98
3	53.6	54.81	59.98
4	64.7	49.59	53.77
5	54.5	54.39	59.48
6	64.7	49.59	53.77

Table 6: Activation and deactivation times using the Umberger Model

11 Forward Simulation

Figure 9 shows the results of a forward simulation using all the above parameters. The total torque supplied at maximal activation, peak moment arms, and peak isometric position show that the model currently is not strong enough to supply the torque required to make the movement.

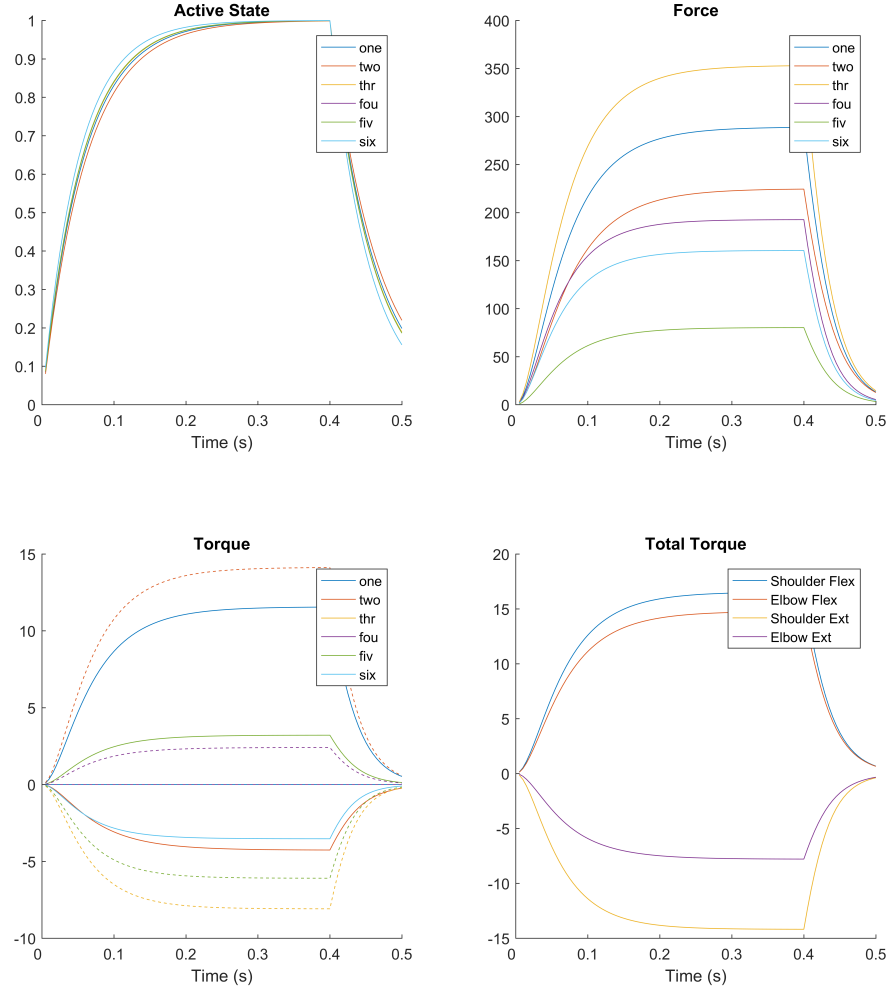


Figure 9: **A.** The active state of the muscles given a neural drive of one. We only see one line here as all the muscles obey the same activation dynamics (10). This could be changed to use the umberger model where we would see slight differences in activation dynamics (12.1.2). **B.** The force output of each muscle given the force-length and force-velocity parameters (9) **C.** Torques supplied by the muscles using momemnt arm x force (8.1). Solid lines are torques about the elbow, dashed lines about the shoulder. **D** Total torques about each joint.

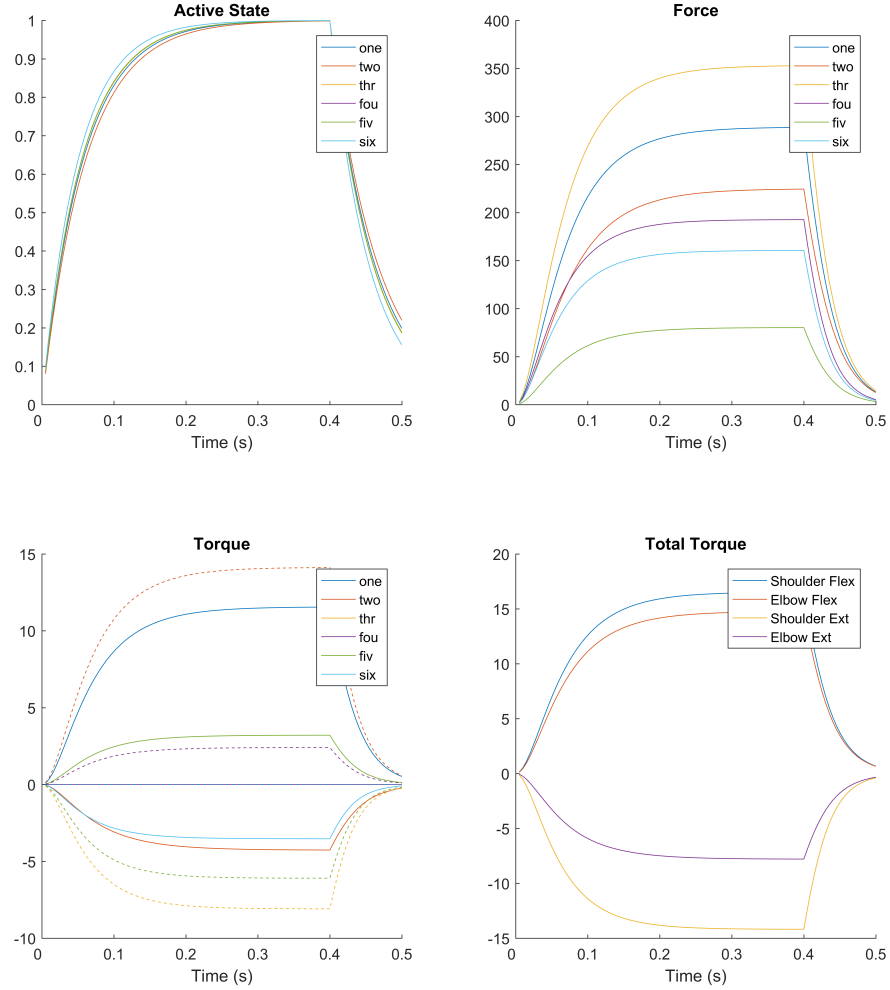


Figure 10: **A.** The active state of the muscles given a neural drive of one. The activation dynamics are from the umberger model so we see slight differences in activaion times (10). This could be changed to use the umberger model where we would see slight differences in activation dynamics (12.1.2,12.1.2). **B.** The force output of each muscle given the force-length and force-velocity parameters (9) **C.** Torques supplied by the muscles using momemnt arm \times force (8.1). Solid lines are torques about the elbow, dashed lines about the shoulder. **D** Total torques about each joint.

12 Umberger Energy Model

This model is used for a multitude of models to estimate the energy expenditure of muscles[33]. It is not clear how well this can predict the absolute energy expenditure, but I've been told it is good for comparing between groups.

12.1 Mechanical Muscle Model

12.1.1 Hill Constants

This model uses a modified Hill-Type model. It was modified to better account for force production at submaximal activation and the effects of between-muscle fibre type differences. Consisted of a contractile element(CE) and a series elastic element (SEE).

The normalized hill constant $A_{REL}(= a/F_{MAX})$ and $B_{REL}(= b/L_{CE(OPT)})$ determine the shape of force-velocity curve and maximal shortening velocity (and power that can be generated given maximal isometric force (F_{MAX})). Multiple muscles are modeled simultaneously, the common approach is to assign all muscles same normalized Hill-constants. Here, they scale A_{REL} and B_{REL} by the percent of fast twitch fibers.

$$A_{REL} = 0.1 + 0.4(\%FT/100) \quad (17)$$

$$B_{REL} = A_{REL}\tilde{V}_{CE(MAX)}$$

In these constants, $\tilde{V}_{CE} = V_{CE}/L_{CE(OPT)}$, and is expressed in $L_{CE(OPT)}s^{-1}$. A value of 12 $L_{CE(OPT)}s^{-1}$ is used for $\tilde{V}_{CE(MAX)}$.

12.1.2 Activation Dynamics

Delays between STIM and ACT were modeled as a first-order process. We use a relation for τ_{ACT} and τ_{DEACT} :

$$\tau_{ACT} = 80\text{ms} - 0.47\text{ms} \times \%FT \quad (18)$$

$$\tau_{DEACT} = 90\text{ms} - 0.56\text{ms} \times \%FT$$

Two rate constants are related to activation and deactivation by the time constants c_1 and c_2 :

$$c_1 = \frac{1}{\tau_{ACT}} - c_2 \quad \text{and} \quad c_2 = \frac{1}{\tau_{DEACT}} \quad (19)$$

The time constants are scaled as well by the percent of fast twitch motor units. We assume that the ratio of $V_{CE(MAX)}$ for FT to ST fibers is 2.5:1. The activation dynamics is then modeled as a first order differential equation Eq. 20.

$$\begin{aligned} \dot{a}(t) &= (u(t) - a(t)) (c_1 u(t) + c_2) \\ \dot{a}(t) &= (u(t) - a(t)) \left(u(t) \left[\frac{1}{\tau_{ACT}} - \frac{1}{\tau_{DEACT}} \right] + \frac{1}{\tau_{DEACT}} \right) \\ \dot{a}(t) &= (u(t) - a(t)) \left(\frac{u(t)}{\tau_{ACT}} - \frac{u(t) - 1}{\tau_{DEACT}} \right) \end{aligned} \quad (20)$$

I was trying to simplify this to look like Eq. 16 but couldn't figure it out quickly so I kept going.

12.1.3 Mechanical to thermal energy estimates

We need to compute muscle masses to convert between these two variables.

$$F_{MAX} = \sigma \text{PCSA} \quad (21)$$

Where σ is the specific tension of the muscle in Pa and PCSA is in m^2 . σ in the Umberger model is 0.25 MPa, or 25E4 Pa.

The muscle mass (kg) is calculated:

$$\text{mass} = \text{PCSA} \rho L_{CE(OPT)} \quad (22)$$

$\rho = 1059.7 \text{ kg/m}^3$ and $L_{CE(OPT)}$ is in m.

12.2 Energy Expenditure Model

$$\dot{E} = \dot{h}_A + \dot{h}_M + \dot{h}_{SL} + \dot{w}_{CE} \quad (23)$$

12.2.1 Activation and Maintenance Heat Rate

$$\dot{h}_{AM} = 1.28 \times \%FT + 25 \quad (24)$$

About 40% of \dot{h}_{AM} is attributed to activation, the other 60% is maintenance.

12.2.2 Shortening Muscle

Shortening heat coefficients for ST and FT fibers:

$$\begin{aligned}\alpha_{S(ST)} &= \frac{4 \times 25}{\tilde{V}_{CE(MAX-ST)}} \\ \alpha_{S(FT)} &= \frac{1 \times 153}{\tilde{V}_{CE(MAX-FT)}}\end{aligned} \quad (25)$$

For these coefficients, $\tilde{V}_{CE(MAX-FT)}$ is defined by the Hill coefficients A_{REL} and B_{REL} . $\tilde{V}_{CE(MAX-FT)}$ is assumed to be 2.5 times greater than $\tilde{V}_{CE(MAX-ST)}$

Combining these equations we get the shortening heat rate:

$$\dot{h}_{SL} = -\alpha_{S(ST)}\tilde{V}_{CE}(1 - \%FT/100) - \alpha_{S(FT)}\tilde{V}_{CE}(\%FT/100) \quad \text{for } \tilde{V}_{CE} \leq 0 \quad (26)$$

The first term on the RHS cannot exceed $100 \frac{W}{kg}$.

12.2.3 Lengthening Muscle

The rate of extra heat production in lengthening can be represented as a product of a coefficient α_L and CE velocity, with a slope slightly greater than shortening.

$$\alpha_L = 4\alpha_{S(ST)} \quad (27)$$

Where $\alpha_{S(ST)}$ is defined in equation 3. We then get the heat rate for a lengthening muscle.

$$\dot{h}_{SL} = \alpha_L \tilde{V}_{CE} \quad \text{for } \tilde{V}_{CE} \geq 0 \quad (28)$$

12.2.4 Mechanical Work Rate

Mass specific mechanical work rate is given by:

$$\dot{w}_{CE} = -\frac{F_{CE}V_{CE}}{m} \quad (29)$$

Where m is the mass of the muscle.

12.2.5 Scaling Factors

Scaling factors needed to be added to account for the length and activation dependence of \dot{h}_{AM} and \dot{h}_{SL} . \dot{h}_M and \dot{h}_{SL} are scaled by the noromalized, isometric force-length relation (F_{iso}) when $L_{CE} > L_{CE(OPT)}$. To get appropriate activation dependence a scaling factor (A) that depends on STIM and ACT is defined:

$$A = \begin{cases} STIM & \text{when } STIM > ACT \\ (STIM + ACT)/2 & \text{when } STIM \leq ACT \end{cases} \quad (30)$$

Then for scaling \dot{h}_{AM} and \dot{h}_{SL} we define:

$$\begin{aligned} A_{AM} &= A^{0.6} \\ A_S &= A^{2.0} \end{aligned} \quad (31)$$

\dot{h}_{SL} is scaled by A_S when $\tilde{V}_{CE} \leq 0$ and by A when $\tilde{V}_{CE} > 0$.

12.3 Total Energy Rate

The total energy liberation for a muscle in W/kg (total muscle mass) is:

$$\begin{aligned} &\text{if } L_{CE} \leq L_{CE(OPT)} \\ \dot{E} &= \dot{h}_{AM} A_{AM} S \\ &+ \begin{cases} [-\alpha_{S(ST)} \tilde{V}_{CE} (1 - \%FT/100) - \alpha_{S(FT)} \tilde{V}_{CE} (\%FT/100)] \cdot A_S S & \text{if } \tilde{V}_{CE} \leq 0 \\ \alpha_L \tilde{V}_{CE} A_S S & \text{if } \tilde{V}_{CE} > 0 \\ -(F_{CE} V_{CE})/m \end{cases} \end{aligned} \quad (32)$$

$$\begin{aligned} &\text{if } L_{CE} > L_{CE(OPT)} \\ \dot{E} &= (0.4 \times \dot{h}_{AM} + 0.6 \times \dot{h}_{AM} F_{ISO} A_{AM} S) \\ &+ \begin{cases} [-\alpha_{S(ST)} \tilde{V}_{CE} (1 - \%FT/100) - \alpha_{S(FT)} \tilde{V}_{CE} (\%FT/100)] F_{ISO} A_S S & \text{if } \tilde{V}_{CE} \leq 0 \\ \alpha_L \tilde{V}_{CE} F_{ISO} A_S S & \text{if } \tilde{V}_{CE} > 0 \\ -(F_{CE} V_{CE})/m \end{cases} \end{aligned} \quad (33)$$

13 Metabolic Methods

For the first experiment, seated subjects made horizontal arm reaching movements using a robotic arm manipulandum (Interactive Motion Technologies Shoulder-Elbow Robot 2) while secured to a chair by a 4-point seatbelt. The position of the handle controlled a cursor on a computer screen that was placed just above head level and about 3 feet in front of the subject. Visual feedback was provided to the subjects throughout the experiment. To begin a trial subjects would need to hold the cursor within the home location for 200 ms. The home circle would then disappear and a target circle 10 cm away would appear. The target would appear randomly at 45, 135, 225, and 315 degrees randomly. Subjects were trained to move at designated speeds with a 100 ms time window. If subjects moved too fast the target circle would turn grey, where if the subject moved to quickly the target would turn green. Making the movement within the time window caused the target to ‘explode’ and turn yellow and play an auditory tone. Once completing an outward reaching trial, the home and target circle locations would swap and the subject would make another reaching movement towards the center of the screen. A subject would go through all four

targets in a pseudorandom order then begin the process again. Subjects would make arm reaching movements for 5 minutes while collecting metabolic data approximately every 5 seconds (Parvomedics system). They went through four different mass conditions and six different speeds. The completed mass conditions were 0, 5, 10, and 20 lbs of added mass at the robot handle. The effective mass of a typical human arm CITE and robot arm in these four mass conditions were about 2.5, 4.5, 6.5, and 10.4 kg. The different speed conditions ranged from 0.4 s – 1.3 s. The numbers of trials per block were calculated for 5 minutes of reaching. The speeds were: Very, Very Slow (VVS, 1.3 s, 160 trials), Very Slow (VS, 1.1 s, 170 trials), Slow (S, 0.9 s, 200 trials), Medium (M, 0.7 s, 220 trials), Fast (F, 0.5 s, 240 trials), Very Fast (VF, 0.375s, 250 trials), and Very, Very Fast (VVF, 0.25s, 260 trials). DON'T THINK TIMES ARE CORRECT CITE

Because the effect of arm reaching on metabolic cost is much smaller compared to walking or cycling subjects were required to be well rested before testing. Testing sessions began with the subject sitting in the chair for 10 minutes. A baseline reading was then taken for 5 minutes and 3 times. Participants then began the arm reaching trials. Subjects rested between each block for 5 minutes to adjust back to baseline. The metabolic energy was calculated in joules per second, \dot{e} , using the method described by Brockway (Brockway, 1987):

$$\dot{e} = 16.58\dot{V}_{O_2} + 4.51\dot{V}_{CO_2} \quad (34)$$

Seated metabolic rate was subtracted from gross metabolic rate to determine the metabolic rate associated with the reaching movement only. After data was collected using custom MATLAB scripts were used to parse the data by trial, mass, and speed. Movement related variables were calculated using these scripts such as velocity, movement duration, reaction time, and metabolic cost of the movement were calculated.

14 Model Fitting

Five predictor variables were extracted from the model simulations for all the simulations (minimization parameter, target, speed, mass condition). The five variables were joint torque, muscle force, active state, neural drive, and the Umberger energy model. These variables were summed across the 4 targets then averaged to get our predictor variable for a given condition and speed. The predictor was then fit to collected metabolic cost data in a simple linear or 'free' manner. The simple equations are shown in equation 35 where a, b, and c are fit depending on the fitting method used.

$$\begin{aligned} Met &= ax + b \text{ Linear Case} \\ Met &= ax^c + b \text{ Free Case} \end{aligned} \quad (35)$$

This was done for each predictor variable and each minimization function. Next R^2 values were computed using the fits and AIC and BIC can be used here to determine the best model fits. More complicated models could be fit but currently we want to keep it simple.

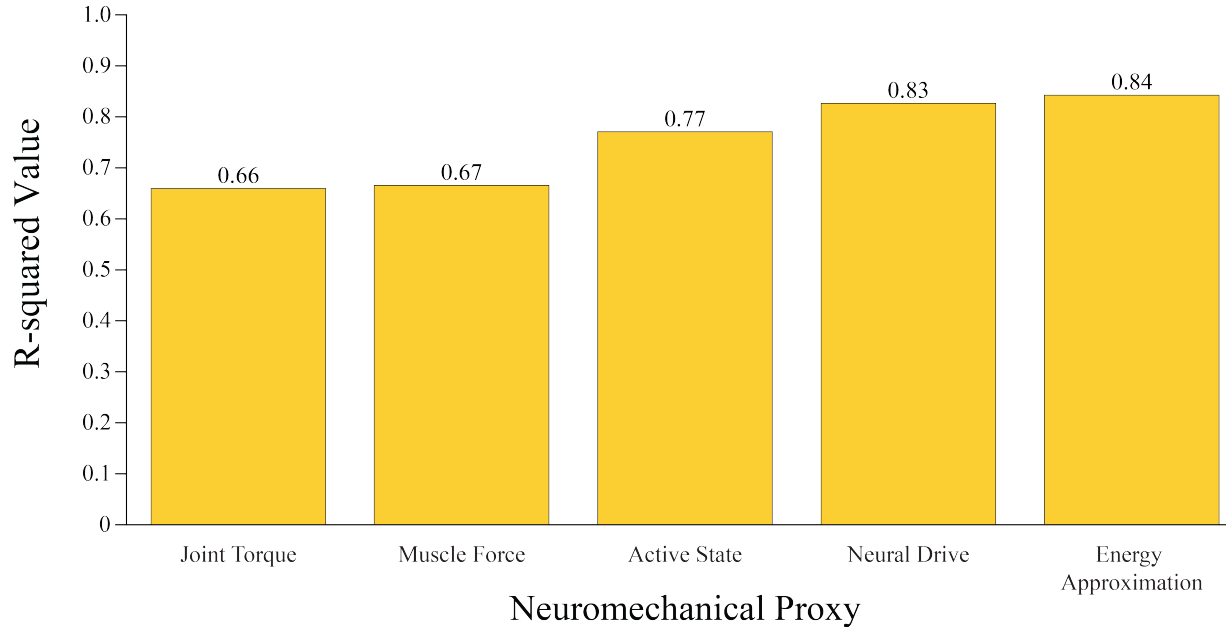
15 Results

Computed R^2 values can be seen in fig 11 and fig 12. The peak R^2 value for the linear case comes from minimizing stress and using the Umberger model as the prediction with an R^2 value of 0.71. In the free case minimizing stress and using the Umberger model again has the highest R^2 value at 0.72. It looks like across all the model fits the Umberger Model does the best at explaining metabolic cost of reaching and then joint torque.

The best linear fit for this model was using the Umberger energy expenditure model minimizing force. This gave an R^2 value of 0.71 with a model fit equation as shown in equation 36 where x is the predictor variable (Umberger Energy model). How this model compares to the collected metabolic data is shown in figure 13.

$$\dot{e} = 3.25 \cdot x - 25.11 \quad (36)$$

A



B

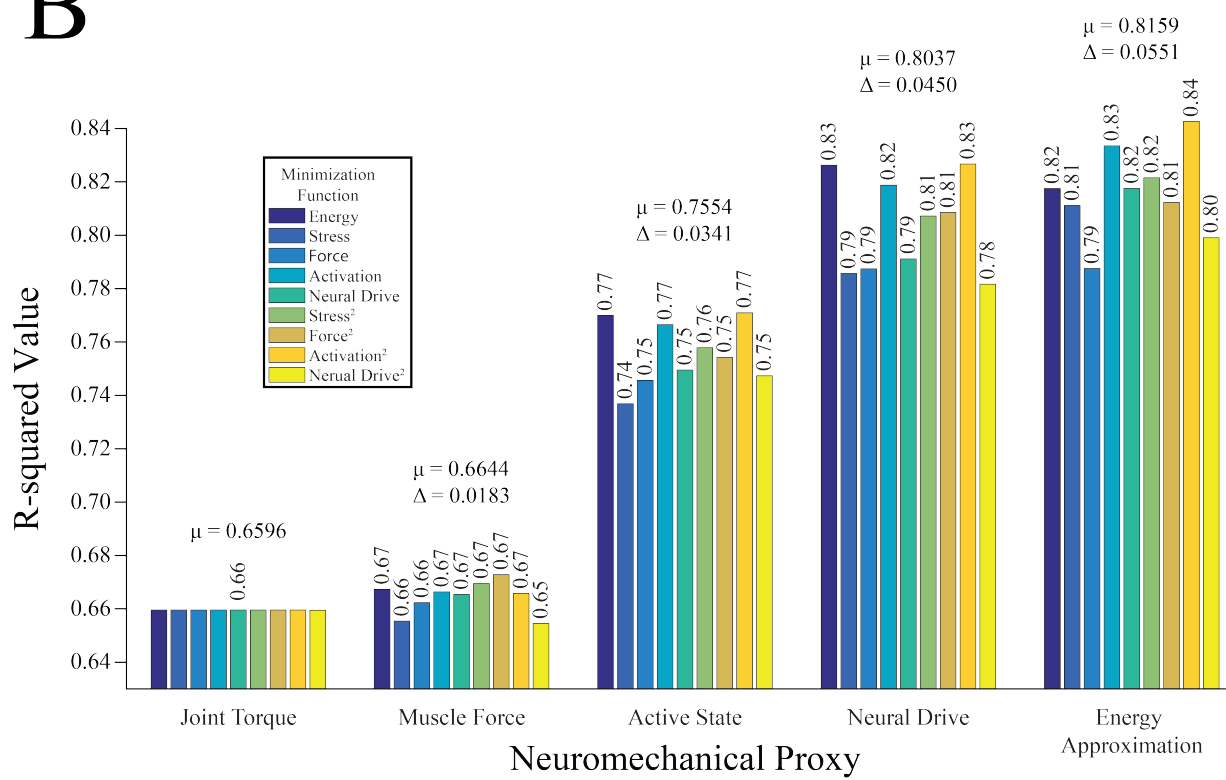


Figure 11: R^2 value as a function of minimization parameter and predictor variable for a linear fit.

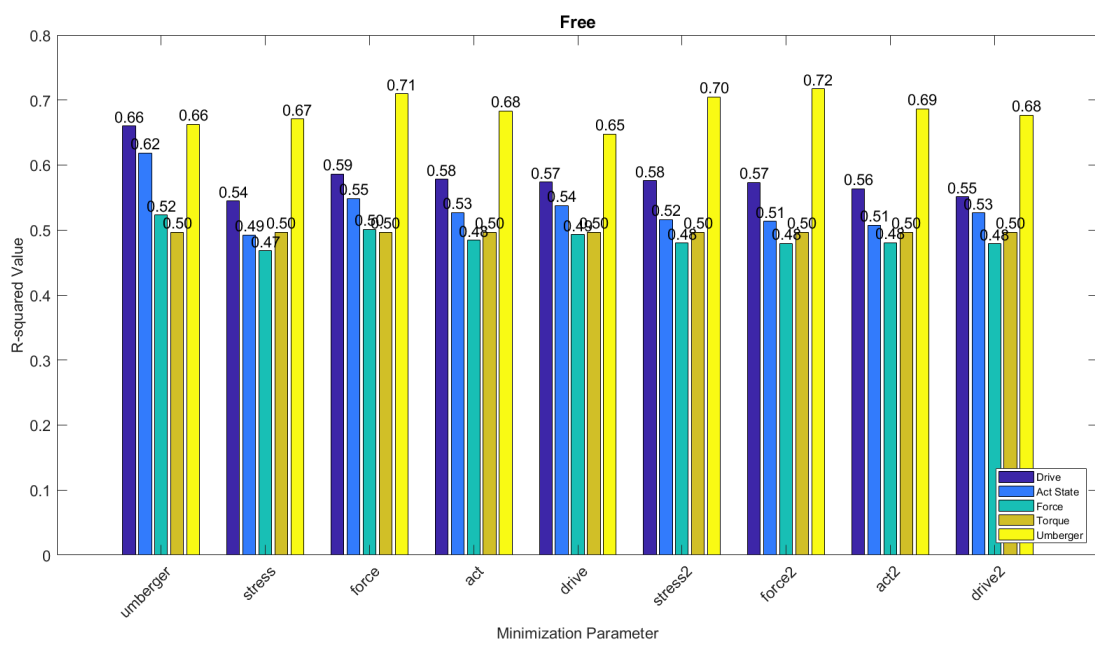


Figure 12: R^2 value as a function of minimization parameter and predictor variable for an exponential fit.

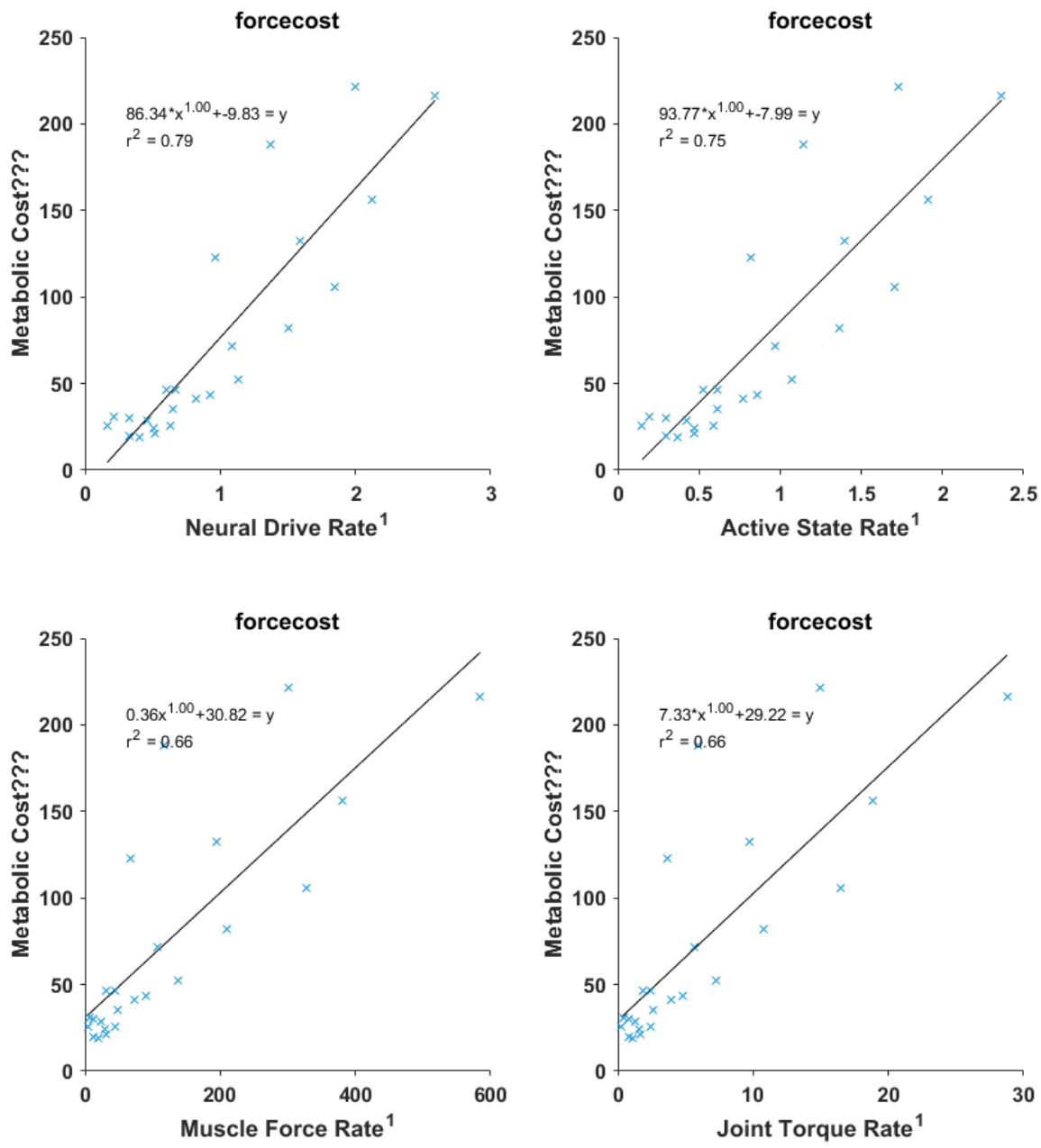


Figure 13: A. Model compared to metabolic cost with R^2 and model fit equation. B. The model fit compared to the collected metabolic cost.

16 References

- [1] Yi-Wen Chang, Fong-Chin Su, Hong-Wen Wu, and Kai-Nan An. Optimum length of muscle contraction. *Clinical Biomechanics*, 14(8):537–542, October 1999.
- [2] Joseph Langenderfer, Seth A. Jerabek, Vijay B. Thangamani, John E. Kuhn, and Richard E. Hughes. Musculoskeletal parameters of muscles crossing the shoulder and elbow and the effect of sarcomere length sample size on estimation of optimal muscle length. *Clinical Biomechanics (Bristol, Avon)*, 19(7):664–670, August 2004.
- [3] Wendy M. Murray, Thomas S. Buchanan, and Scott L. Delp. The isometric functional capacity of muscles that cross the elbow. *Journal of Biomechanics*, 33(8):943–952, August 2000.
- [4] Reza Shadmehr, Helen J. Huang, and Alaa A. Ahmed. A Representation of Effort in Decision-Making and Motor Control. *Current Biology*, 26(14):1929–1934, July 2016.
- [5] S. Adewusi, S. Rakheja, and P. Marcotte. Biomechanical models of the human hand-arm to simulate distributed biodynamic responses for different postures. *International Journal of Industrial Ergonomics*, 42(2):249–260, March 2012.
- [6] Kun Hwang, Jin Yi Han, and In Hyuk Chung. Topographical Anatomy of the Anconeus Muscle for Use as a Free Flap. *Journal of Reconstructive Microsurgery*, 20(08):631–636, November 2004.
- [7] J. Fridén, D. Albrecht, and R. L. Lieber. Biomechanical analysis of the brachioradialis as a donor in tendon transfer. *Clinical Orthopaedics and Related Research*, (383):152–161, February 2001.
- [8] W. Li and E. Todorov. Iterative linearization methods for approximately optimal control and estimation of non-linear stochastic system. *International Journal of Control*, 80(9):1439–1453, September 2007.
- [9] Katherine R. S. Holzbaur, Wendy M. Murray, and Scott L. Delp. A Model of the Upper Extremity for Simulating Musculoskeletal Surgery and Analyzing Neuromuscular Control. *Annals of Biomedical Engineering*, 33(6):829–840, June 2005.
- [10] Pascale Pigeon, L’Hocine Yahia, and Anatol G. Feldman. Moment arms and lengths of human upper limb muscles as functions of joint angles. *Journal of Biomechanics*, 29(10):1365–1370, October 1996.
- [11] E. J. van Zuylen, A. van Velzen, and J. J. Denier van der Gon. A biomechanical model for flexion torques of human arm muscles as a function of elbow angle. *Journal of Biomechanics*, 21(3):183–190, January 1988.
- [12] Dinant A. Kistemaker, Arthur J. (Knoek) Van Soest, and Maarten F. Bobbert. A model of open-loop control of equilibrium position and stiffness of the human elbow joint. *Biological Cybernetics*, 96(3):341–350, March 2007.
- [13] Raja Dahmane, Srdjan Djordjević, Bostjan Šimunić, and Vojko Valenčič. Spatial fiber type distribution in normal human muscle: Histochemical and tensiomyographical evaluation. *Journal of Biomechanics*, 38(12):2451–2459, December 2005.
- [14] M. A. Johnson, J. Polgar, D. Weightman, and D. Appleton. Data on the distribution of fibre types in thirty-six human muscles: An autopsy study. *Journal of the Neurological Sciences*, 18(1):111–129, January 1973.
- [15] I. E. Brown, E. J. Cheng, and G. E. Loeb. Measured and modeled properties of mammalian skeletal muscle. II. The effects of stimulus frequency on force-length and force-velocity relationships. *Journal of Muscle Research and Cell Motility*, 20(7):627–643, October 1999.
- [16] Wendy M. Murray, Scott L. Delp, and Thomas S. Buchanan. Variation of muscle moment arms with elbow and forearm position. *Journal of Biomechanics*, 28(5):513–525, May 1995.
- [17] Dinant A. Kistemaker, Jeremy D. Wong, and Paul L. Gribble. The Central Nervous System Does Not Minimize Energy Cost in Arm Movements. *Journal of Neurophysiology*, 104(6):2985–2994, December 2010.

- [18] S. L. Delp, J. P. Loan, M. G. Hoy, F. E. Zajac, E. L. Topp, and J. M. Rosen. An interactive graphics-based model of the lower extremity to study orthopaedic surgical procedures. *IEEE Transactions on Biomedical Engineering*, 37(8):757–767, August 1990.
- [19] T. Flash and N. Hogan. The coordination of arm movements: an experimentally confirmed mathematical model. *Journal of Neuroscience*, 5(7):1688–1703, July 1985.
- [20] Rainer Hessmer. Kinematics for Lynxmotion Robot Arm, October 2009.
- [21] Reza Shadmehr. Computational Neurobiology of Reaching and Pointing A Foundation for Motor Learning, 2005.
- [22] E Eisenberg, T L Hill, and Y Chen. Cross-bridge model of muscle contraction. Quantitative analysis. *Biophysical Journal*, 29(2):195–227, February 1980.
- [23] George I. Zahalak and Shi-Ping Ma. Muscle Activation and Contraction: Constitutive Relations Based Directly on Cross-Bridge Kinetics. *Journal of Biomechanical Engineering*, 112(1):52–62, February 1990.
- [24] H. Hatze. A myocybernetic control model of skeletal muscle. *Biological Cybernetics*, 25(2):103–119, June 1977.
- [25] J. M. Winters and L. Stark. Muscle models: what is gained and what is lost by varying model complexity. *Biological Cybernetics*, 55(6):403–420, 1987.
- [26] Marcelo Epstein and Walter Herzog. *Theoretical Models of Skeletal Muscle: Biological and Mathematical Considerations*. 1998.
- [27] N P Whitehead, N S Weerakkody, J E Gregory, D L Morgan, and U Proske. Changes in passive tension of muscle in humans and animals after eccentric exercise. *The Journal of Physiology*, 533(Pt 2):593–604, June 2001.
- [28] Katherine R. S. Holzbaur, Scott L. Delp, Garry E. Gold, and Wendy M. Murray. Moment-generating capacity of upper limb muscles in healthy adults. *Journal of Biomechanics*, 40(11):2442–2449, January 2007.
- [29] Le Li, Kaiyu Tong, Rong Song, and Terry K. K. Koo. Is maximum isometric muscle stress the same among prime elbow flexors? *Clinical Biomechanics*, 22(8):874–883, October 2007.
- [30] R. Horowitz. Passive force generation and titin isoforms in mammalian skeletal muscle. *Biophysical Journal*, 61(2):392–398, February 1992.
- [31] Jack M. Winters. An improved muscle-reflex actuator for use in large-scale neuromusculoskeletal models. *Annals of biomedical engineering*, 23(4):359–374, 1995.
- [32] Darryl G. Thelen. Adjustment of Muscle Mechanics Model Parameters to Simulate Dynamic Contractions in Older Adults. *Journal of Biomechanical Engineering*, 125(1):70–77, February 2003.
- [33] Brian R. Umberger, Karin. G. M. Gerristen, and Philpe. E. Martin. A Model of Human Muscle Energy Expenditure. *Computer Methods in Biomechanics and Biomedical Engineering*, 6(2):99–111, May 2003.